Wiley
International Journal of Corrosion
Volume 2024, Article ID 5591969, 17 pages
https://doi.org/10.1155/2024/5591969

Research Article

Pitting Corrosion of Austenitic Stainless Steels in Electroactivated Water

Benjamín Valdez-Salas,[1,2] **Jorge Salvador-Carlos**,[1,2] **Ernesto Beltrán-Partida**,[1] **Mario Alberto Curiel-Álvarez**,[1] **Ernesto Valdez-Salas**,[1] **and Nelson Cheng**[2]

[1]*Core Facility de Química y Materiales Avanzados, Instituto de Ingeniería, Universidad Autónoma de Baja California, Blvd. Benito Juárez and Normal s/n, Mexicali, Baja California 21280, Mexico*
[2]*Magna International Pte Ltd, 10H Enterprise Road, Singapore 692834, Singapore*

Correspondence should be addressed to Jorge Salvador-Carlos; jsalvador@uabc.edu.mx

Received 29 May 2024; Accepted 31 July 2024

Academic Editor: Michael J. Schütze

The pitting corrosion behavior of austenitic stainless steels (SSs) UNS S30400 and UNS S31600 exposed to electroactivated water (EAWA) (oxidation–reduction potential [ORP] 1100 ± 15 mV and pH 4.5 ± 0.2) was evaluated by gravimetric tests, linear and cyclic potentiodynamic polarization (CPP), electrochemical impedance spectroscopy (EIS), atomic force microscopy (AFM), scanning electron microscopy (SEM), and energy-dispersive X-ray spectroscopy (EDS). Gravimetric and electrochemical results for corrosion rates indicate a good corrosion resistance of the tested SS. However, localized pitting corrosion appears after 1 week of exposure to EAWA, as was corroborated by the results of both corrosion rate and surface analysis. Special care must be taken for the sanitization of SS surfaces used in medical installations to avoid their corrosion when EAWA is applied as a disinfectant.

Keywords: anolyte; austenitic stainless steel; electroactivated water; pitting corrosion

1. Introduction

Electroactivated water (EAWA), also known as electrochemically activated water or superoxidized water, is a product of a series of subprocesses such as electrolytic deposition, electrophoresis, electroflotation, and electrocoagulation [1]. These subprocesses involve redox reaction ion transport at the anode and cathode with evolving gas and flocculation reactions. The reactions occur in an electrochemical cell with two different environments divided by a semipermeable membrane, in which the cathode contains the alkaline media (catholyte) and the anode the acidic media (anolyte) [2]. For both the catholyte and the anolyte, physicochemical parameters such as pH, oxidation–reduction potential (ORP), and electrical conductivity are dependent on factors such as the amount of water, electrode materials, the concentration of NaCl or HCl, temperature, and applied voltage [3, 4]. Anolyte and catholyte are different in chemical composition and physicochemical parameters, as shown in Figure 1 [5].

The particular physicochemical characteristics and the diversity of chemical components in both anolyte and catholyte also provide particular important properties, making them useful for a diversity of applications [6, 7]. Studies have demonstrated that catholyte has antioxidant, immunostimulant, and cleansing properties, and also promotes tissue regeneration, cellular growth, and division [8]. On the other hand, anolyte has antibacterial, antiviral, antifungal, antiallergenic, and anti-inflammatory properties [9–11]. Interestingly, the active compounds in anolyte stand out for not being toxic to somatic cells and superior organisms. Due to its broad spectrum and easy preparation, the anolyte has been included by the World Health Organization (WHO) for use as a disinfectant, antiseptic, and wound-healing agent during the COVID-19 pandemic in 2021 [12].

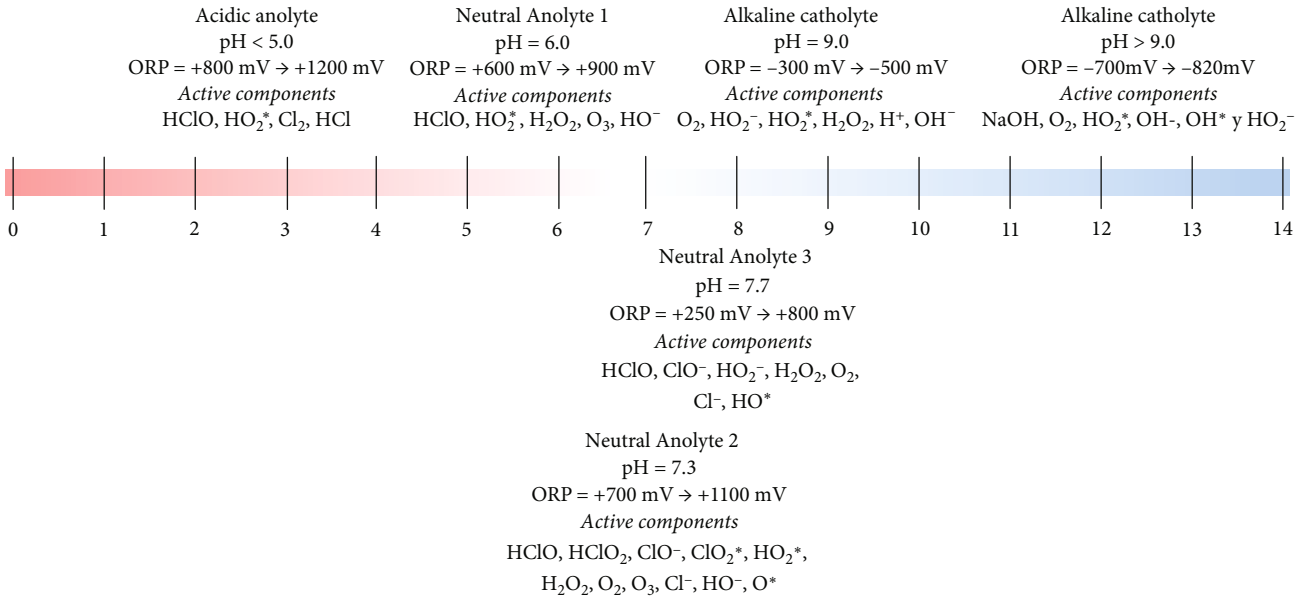

Figure 1: Chemical composition and physicochemical parameters of anolyte and catholyte in function of pH.

From the applications mentioned above, anolyte emerges as a potential solution to current public health problems, such as nosocomial infections and resistance to antimicrobial drugs [13, 14]. However, its inclusion in the market is limited due to its solution stability, which must be improved to reach storage times longer than 6 months, and, most importantly, its corrosive effect that can affect different metallic surfaces such as carbon and stainless steels (SSs) [15, 16]. Regarding its corrosive potential, only a few studies have been published on the corrosiveness of the anolyte on different metallic surfaces. Ayebah and Hung [17] evaluate the corrosion caused by the anolyte (pH: 2.43 ± 0.04; ORP: 1077 ± 67 mV; chlorine concentration: 48.66 ± 1.06 mg/L) on copper, aluminum carbon steel, and SS UNS S30400 and the deterioration of polyvinyl chloride (PVC) for 8 days. The findings showed that all the tested materials, except copper, exhibited a good resistance to corrosion with only a minimum change in the surface roughness. Tanaka et al. [18] studied the corrosiveness of UNS S31600, silicone, propylene, PVC, and rubber exposed for 5 weeks to an anolyte solution (pH: 2.3–2.7; ORP > 1000 mV; chlorine concentration: 10–50 mg/L). After these 5 weeks of exposure, low corrosion rates (0.009 mm/year) were recorded for UNS S31600, but the presence of a pitting attack on the evaluated surfaces was evidenced. These studies highlight the significance of understanding the corrosion behavior of SSs in the anolyte, which are essential alloys used in the food and healthcare industries [19, 20].

Our research presents a corrosion analysis of SSs, UNS S30400 and UNS S31600, which are widely used in the manufacturing of furniture and medical equipment and are exposed to the anolyte of EAWA. Gravimetric, electrochemical, and surface analyses were performed to determine in detail the aggressive corrosion effect of EAWA on the tested SS surfaces and support its inclusion as an efficient, practical, and safe disinfectant.

Table 1: Chemical composition of the SSs, UNS S30400 and UNS S31600, analyzed by LIBS.

	Composition (weight %)							
	Fe	Cr	Mn	Si	Ni	Mo	Cu	Co
UNS S30400	71.5	16.99	1.03	0.76	9.20	—	0.20	0.16
UNS S31600	68.10	16.46	1.42	0.41	10.79	2.21	0.41	0.13

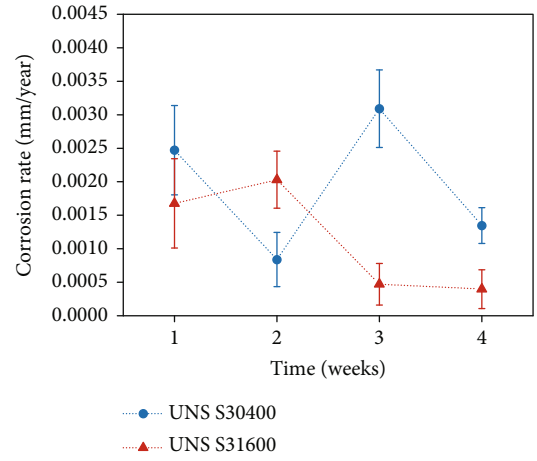

Figure 2: Corrosion rate of UNS S30400 and UNS S31600 exposed to EAWA.

2. Materials and Methods

2.1. Chemical Composition and Surface Preparation of Corrosion Samples. Rectangular samples of cold-rolled UNS S30400 and UNS S31600 with dimensions 2.3 cm wide, 5.5 cm length, and 0.00254 cm thickness were used for the

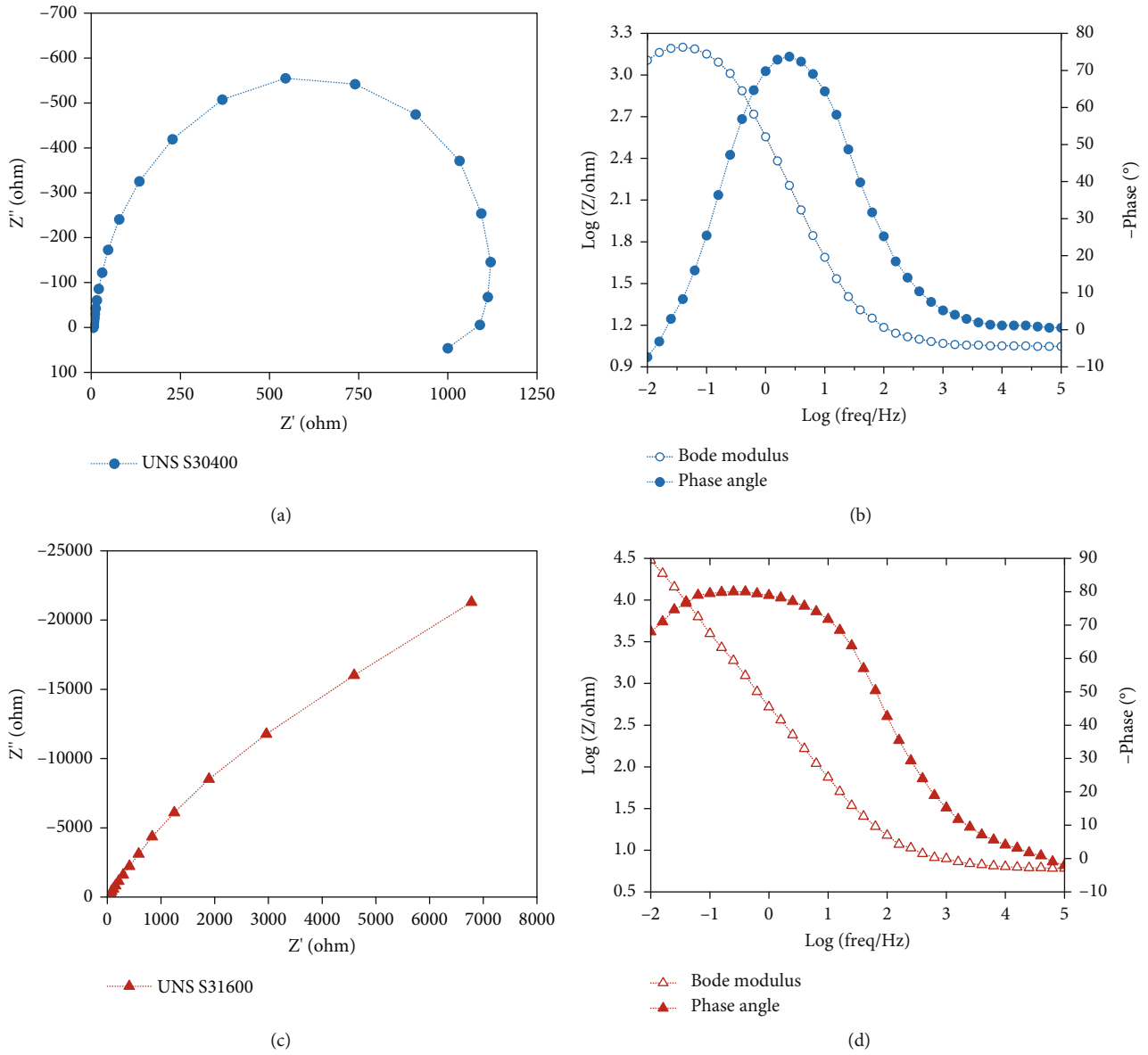

Figure 3: Nyquist and Bode plots: (a, b) UNS S30400 and (c, d) UNS S31600.

gravimetric loss weight tests. The SS samples were polished with SiC emery paper and 0.3 μm alumina to get mirror finishing. For electrochemical tests, 1 cm^2 surface area electrodes were used. The chemical composition of the SS was verified by laser-induced breakdown spectroscopy (LIBS), as shown in Table 1. Before each corrosion test, the samples were rinsed with distilled water and degreased in an ethanol ultrasonic bath for 10 min to remove all the dirt from the surface. Finally, the samples were kept in a desiccator until their exposure to corrosive media.

2.2. EAWA Production. An electrolytic cell (Baoji Ruicheng Titanium Metal Co., Ltd.) with Ru–Ir-coated titanium electrodes was used to produce EAWA. Potential and flow parameters were set to obtain an ORP value of 1100.15 mV and a pH of 4.5 ± 0.2 EAWA from a 0.25% (*w*/*w*) NaCl aqueous solution. The product was stored in high-density polyethylene (HDPE) vessels at room temperature (25 ± 0.5°C).

2.3. Gravimetric Corrosion Tests. SS samples were immersed in 1.2 L of anolyte in an HDPE vessel adapted with plastic holders. The solution remained at 22 ± 1°C and static conditions. The weight loss was recorded weekly for 1 month. Before the weight recording, the samples were cleaned according to ASTM G1-03 [21]. Each gravimetric test was made in triplicate in order to report average values and express the results in millimeters per year using Equation (1) [22].

$$\mathrm{CR} = \frac{\left(3.65 * 10^5\right) W}{\mathrm{ATD}} \quad (1)$$

where CR is the average corrosion rate (millimeters per year), W is the mass loss (grams), A is the exposed surface area of the

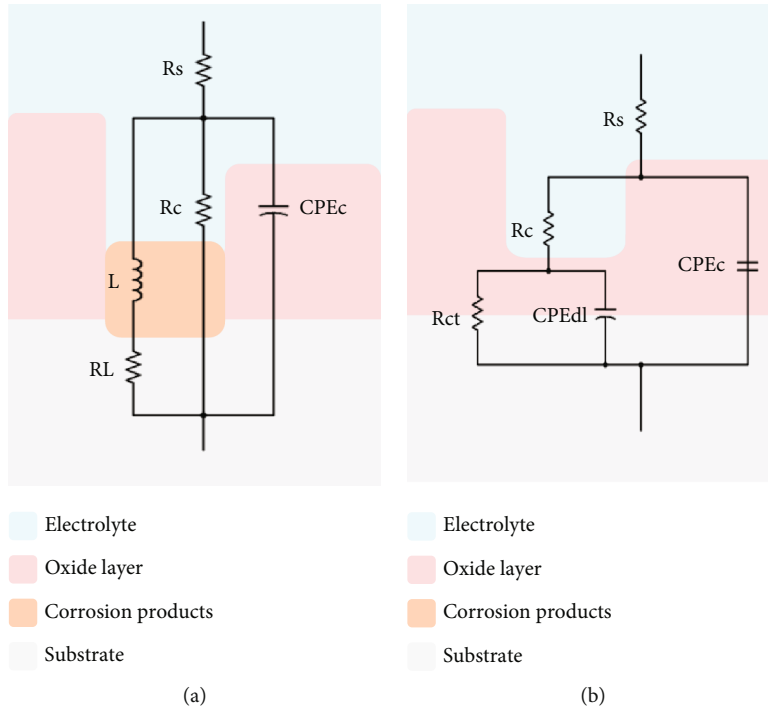

Figure 4: Equivalent circuits of (a) UNS S30400 and (b) UNS S31600.

Table 2: Values of the circuit elements of both SSs.

Sample	Rs (Ω)	Rc (Ω)	CPEc S^* sec^n	Rct (Ω)	CPEdl S^* sec^n	n	RL (Ω)	L (H)	Fit error
SS304	11.63	30.04	5.04e − 05	—	—	—	861.9	0.01933	0.0654
SS316	44.13	23.39	4.12e − 07	3.40e + 11	1.07e − 04	0.7284	—	—	0.0830

sample (square millimeters), T is the exposure time (days), and D is the density of the sample (grams per cubic centimeter).

2.4. Electrochemical Tests. Electrochemical corrosion tests were performed using a potentiostat/galvanostat (CH Instruments Electrochemical Workstation) under static conditions and 22 ± 1°C. The three-electrode electrochemical cell was comprised of a saturated calomel electrode (SCE) as a reference, a platinum counter electrode (CE), and a SS working electrode (WE). The WE with a rectangular shape was supported in acrylic resin to expose a 1 cm^2 surface for analysis. The WE remained immersed in the EAWA solution for a 15-min delay time before each electrochemical test.

Electrochemical impedance spectroscopy (EIS) parameters were set at 6 points per decade in a scan range from 100 KHz to 0.01 Hz and an amplitude of 0.10 mV at open circuit potential conditions. Plots of potentiodynamic polarization (PP) and cyclic PP (CPP) were recorded in triplicate at a 1 mV/s scan rate and a potential range from 0.0 to 0.5 V for UNS S30400 and from 0.0 to 0.7 V for UNS S31600. Corrosion rates were calculated by Tafel analysis using Equation (2), and the average values reported.

$$\mathrm{CR} = \frac{I_{\mathrm{corr}} K E_w}{\rho A} \tag{2}$$

where I_{corr} is the corrosion current (amperes), K is the corrosion rate constant that defines the units (3272 m/A·cm·year), E_w is the equivalent weight (grams per equivalent), ρ is the density (grams per cubic centimeter), and A is the sample area (square centimeters).

2.5. Surface Analysis. Surface morphology changes on surfaces of samples exposed to gravimetric corrosion tests were analyzed by scanning electron microscopy (SEM) and atomic force microscopy (AFM). For SEM and energy-dispersive X-ray spectroscopy (EDS) analysis (SEM-FIB-EDS, Tescan Lyra), the samples were placed in a carbon conductive tape, and analysis was performed at 10 kV with 10 kX. For the AFM analysis (NX-10, Park Systems), the samples were placed in an acoustic shielded box, and the characterization was made using a PPP-NCHR tip. In tapping mode, PPP-NCHR has a constant force of 42 N/m and a resonance frequency of 33 kHz. The scan rate in all samples was 0.8 Hz with an amplitude of 18.79 × 103 mm and an analysis surface area of 100 μm^2.

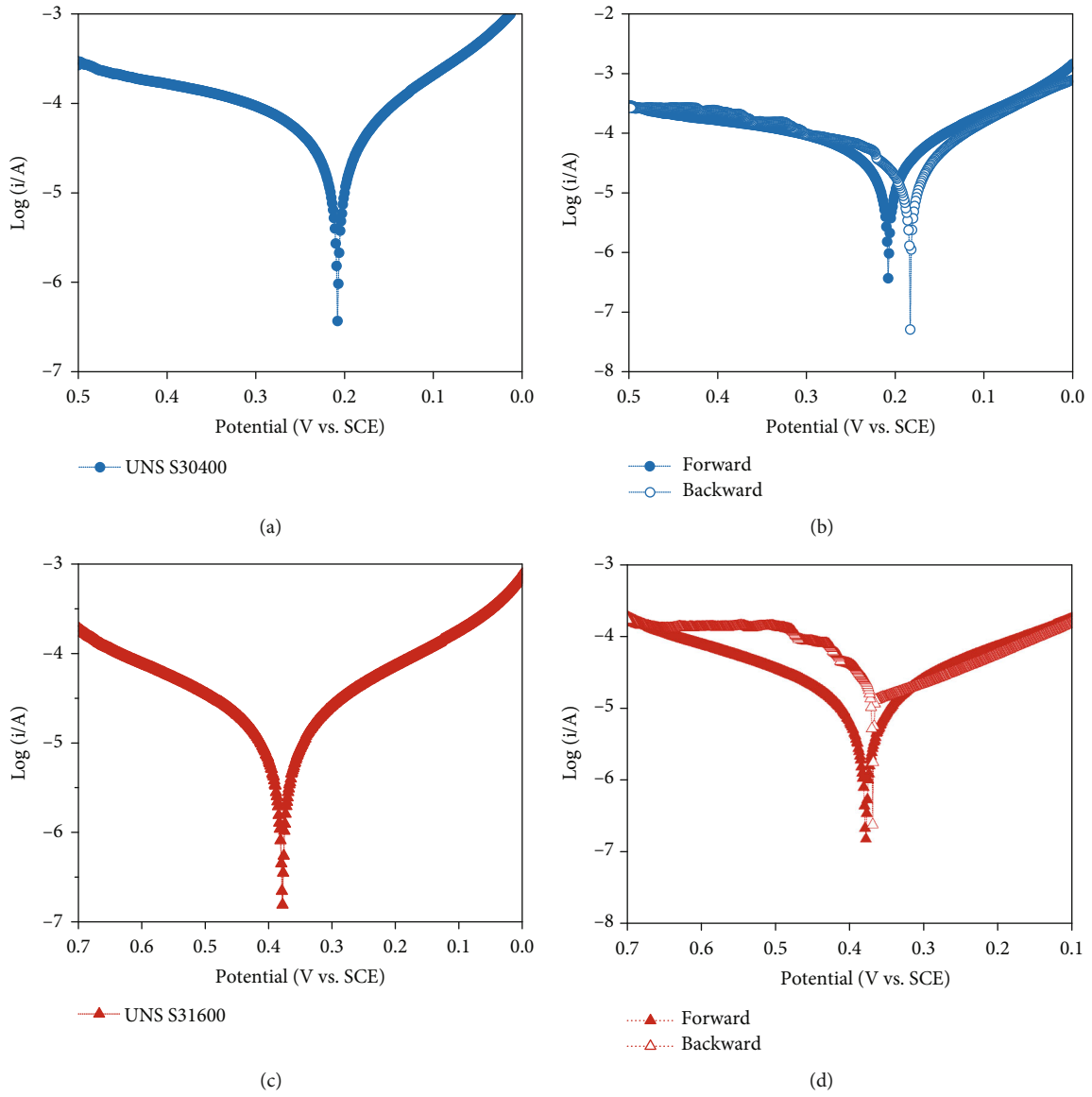

Figure 5: PP and CPP plots: (a, b) UNS S30400 and (c, d) UNS S31600.

Table 3: Electrochemical corrosion parameters for UNS S30400 and UNS S31600 immersed in EAWA.

Sample	E_{corr} (V)	I_{corr} (A)	R_p (Ω)	Cathodic slope (mV/dec)	Anodic slope (mV/dec)	Corrosion rate (mil/year)	Corrosion rate (mm/year)
SS304	0.1990	5.13e − 05	735.70	107.95	118.06	1.337	0.0339
SS316	0.3515	9.65e − 06	4319.65	104.17	121.79	0.254	0.0064

3. Results

3.1. Gravimetric Corrosion Tests. Figure 2 shows the corrosion rate in millimeters per year of the record per week of the gravimetric study of SS coupons immersed in EAWA solutions without stirring. Results for UNS S30400 indicate a trend for continuous weight loss after 4 weeks, discarding any possible passivation of the SS by the oxidative effect of EAWA. On the other hand, samples of UNS S31600 showed a corrosion rate decreasing along the exposure time. It is important to highlight that the corrosion rates obtained in these tests for SS are lower compared to others occurring in corrosive environments containing chloride ions [23–25].

3.2. EIS Results. The Nyquist plots in Figures 3(a) and 3(c) show the electrochemical behavior with a capacitive loop corresponding to a charge transfer reaction during the corrosion process in the interface metal electrolyte. The capacitive loop and the quantity of charge transfer have a linear correspondence. A small value represents the absence of a

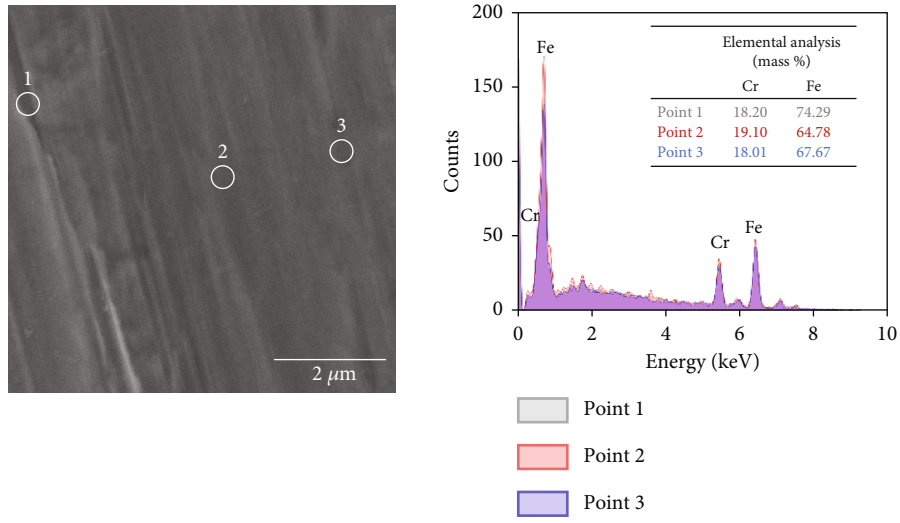

(a)

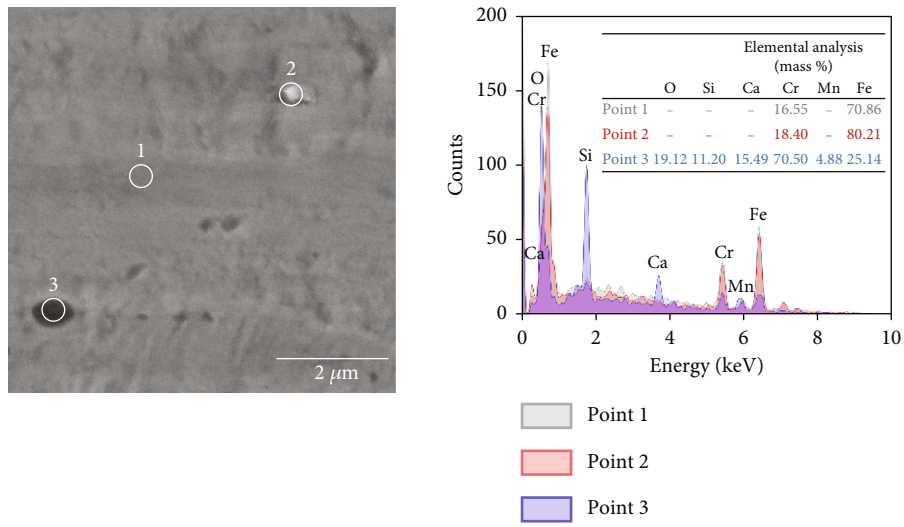

(b)

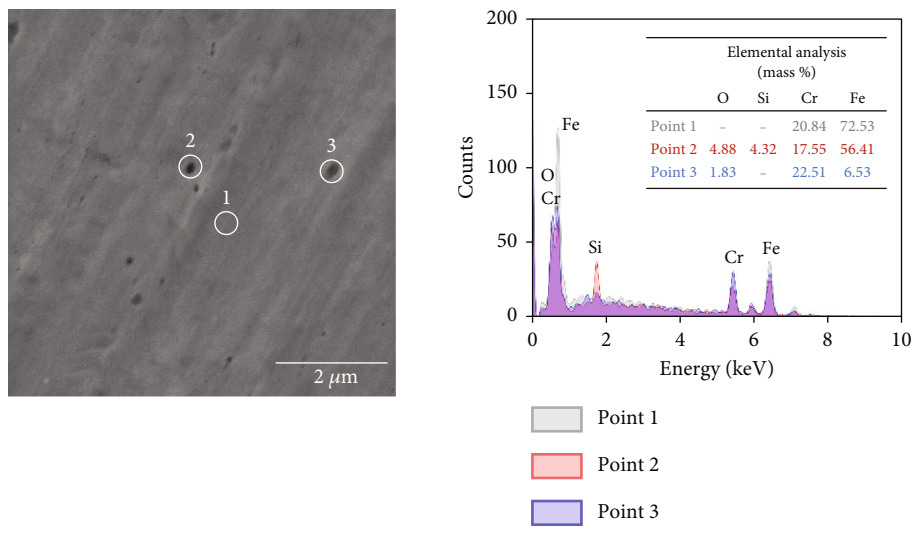

(c)

Figure 6: Continued.

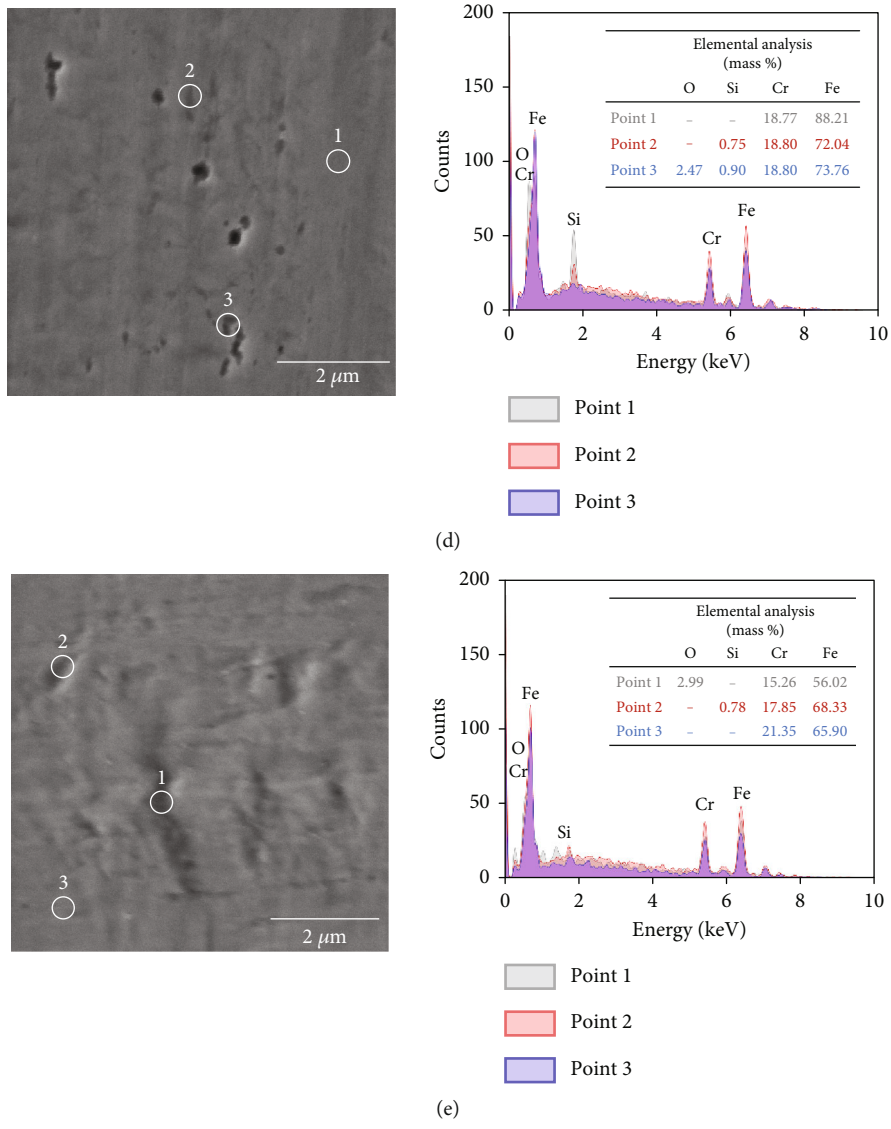

Figure 6: SEM images and EDS spectra of UNS S30400: (a) 0 week, (b) 1 week, (c) 2 weeks, (d) 3 weeks, and (e) 4 weeks of immersion in EAWA.

layer, and the electrons coming from the substrate can freely flow. An increase in the size indicates the formation of a dispersed layer by zones or a highly dense layer, resulting in a diminishing of electron transfer from the metal [26]. For the SSs evaluated in this work, the resistance values (resistance of the oxide layer) are similar to those of the solution and correspond to a dispersed layer.

At low frequencies, the behavior of the SSs is different, showing an inductive response for UNS S30400 and a capacitive one for UNS S31600. The inductive response is interesting because there is no agreement for its explanation, even though it has been expressed as a negative capacitance, where the response of a capacitor is to keep charge, while an inductor or negative capacitor allows the passing of charge [27]. An explanation can be obtained from the relaxing time, which expresses that the metal surface turns back to its initial state (transient valence) due to the presence of metallic ions on the surface [28]. Another explanation related to the mechanism mentioned before is the appearance of active dissolution sites in the metal favored by dislocation in the crystallographic structure, manufacturing failures, or pits [29]. Regarding the capacitive response represented as an incomplete semicircle, we have a diffusive transport of ions or electrolytes through a passive layer or corrosion products on the surface [30].

The phase angle and magnitude Bode plots are shown in Figures 3(b) and 3(d). These plots complement the limitations of Nyquist plots regarding frequencies, especially at low frequencies. The results for UNS S30400 indicate that at low frequencies, the behavior is close to 0°, representing an inductor, while UNS S31600 is close to −90°, behaving as almost an ideal capacitor. It is important to note that the interpretation of these results agrees with what is described in the Nyquist plots, where a difference in the shapes for the SS is also observed. Both SSs have two-time constants, but the first-time constant of UNS S31600 covers

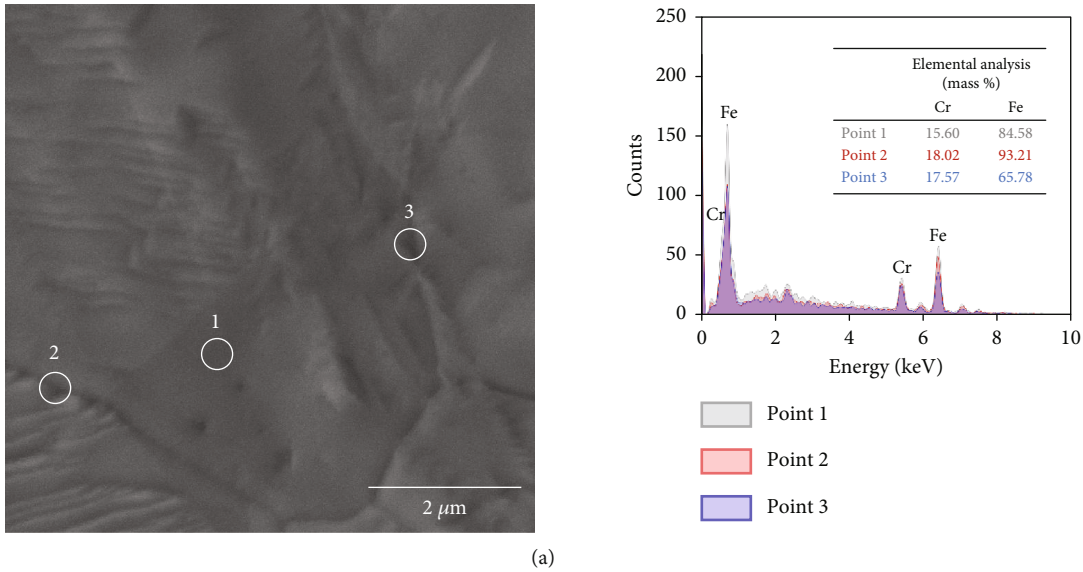

(a)

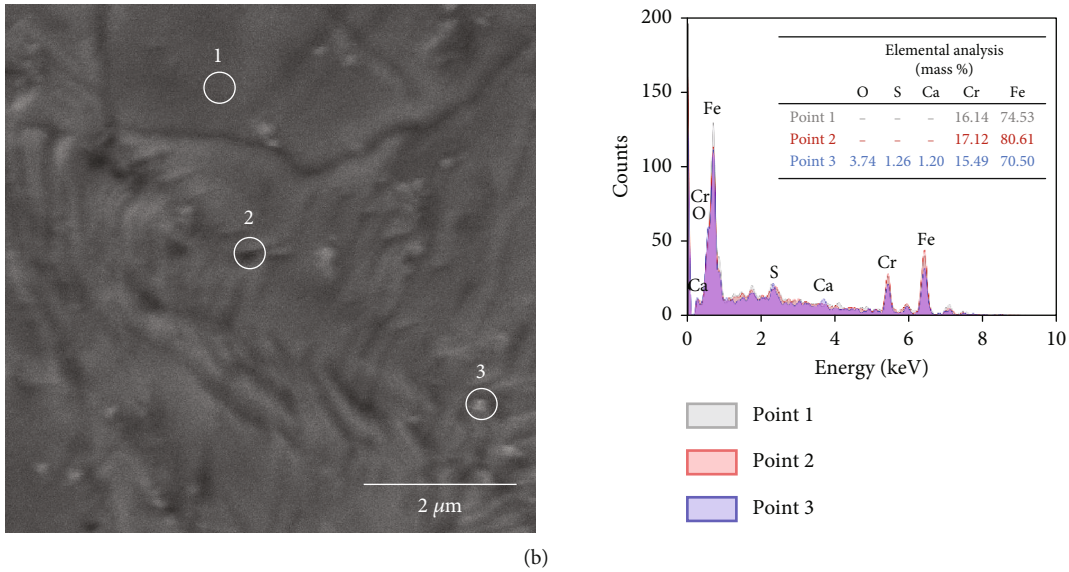

(b)

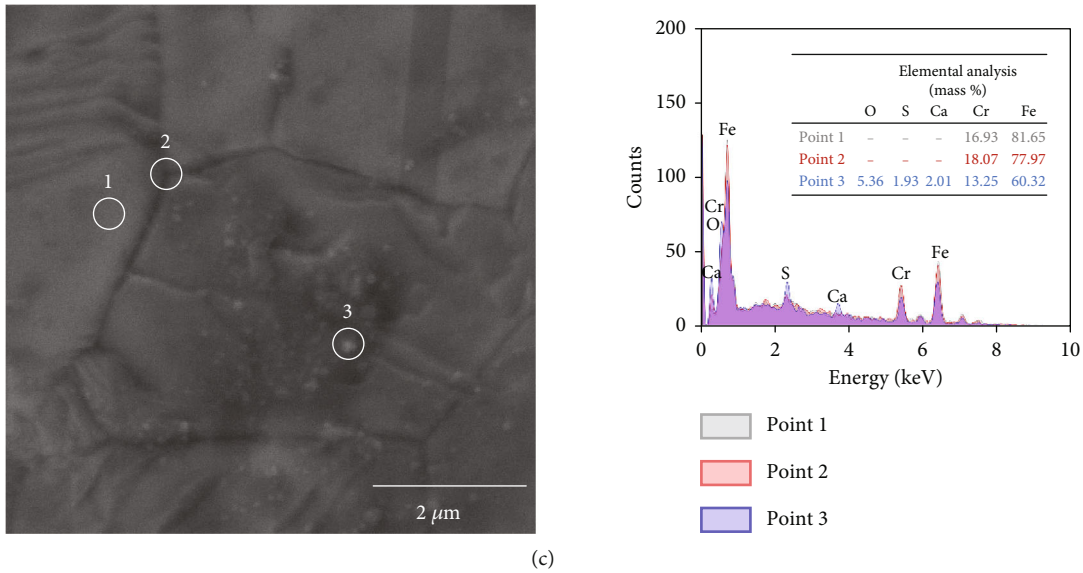

(c)

Figure 7: Continued.

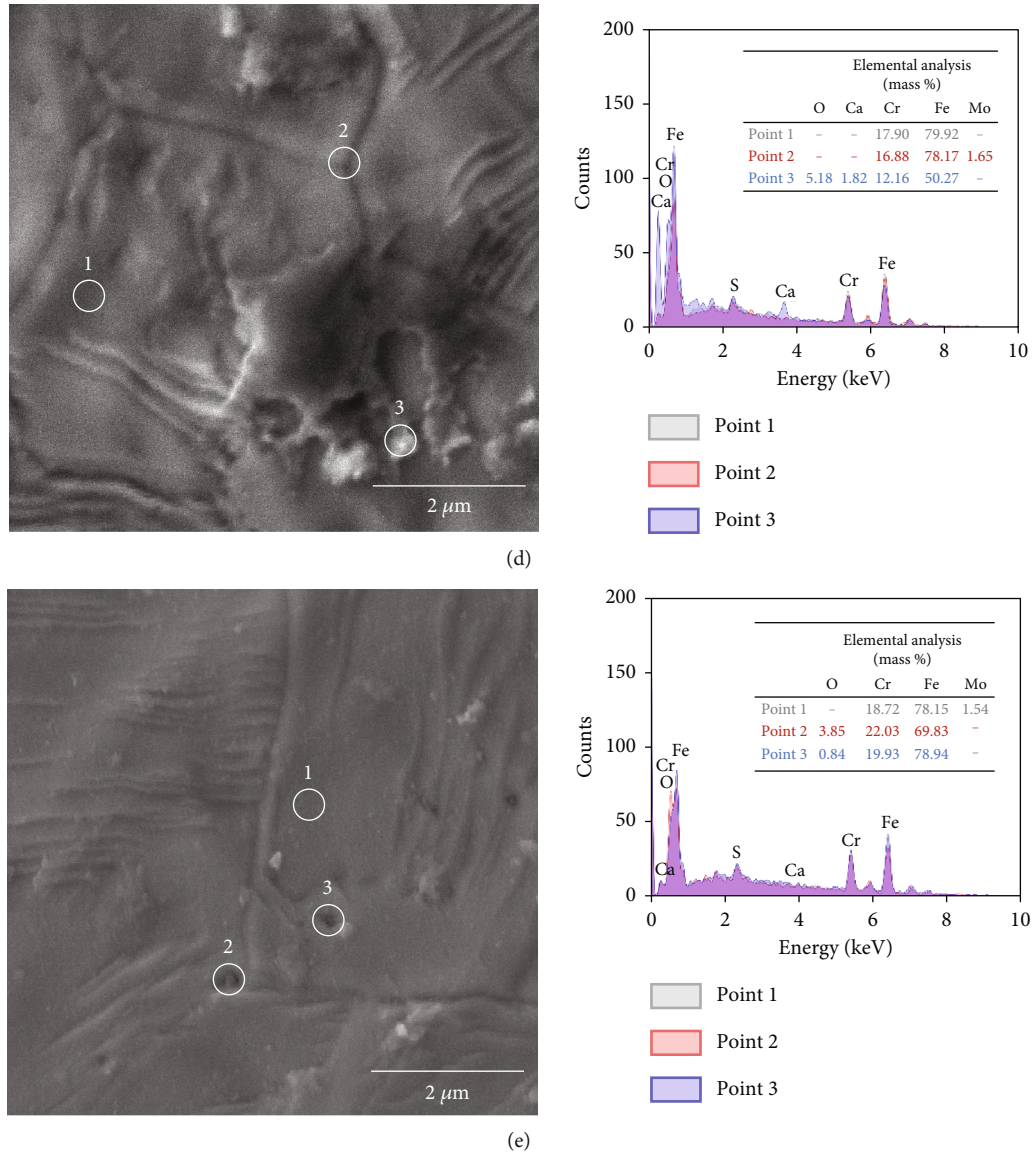

Figure 7: SEM images and EDS spectra of UNS S31600: (a) 0 week, (b) 1 week, (c) 2 weeks, (d) 3 weeks, and (e) 4 weeks of immersion in EAWA.

a greater range. Mainly, these time constants are assigned to the charge transfer processes of the electrons and the native oxide layer. The increase in the range can be associated with a better passive layer in UNS S31600.

Figure 4 shows the different equivalent circuits for both alloys exposed to EAWA solutions to explain the reactions that occurred at the interface. For UNS S30400 (Figure 4(a)), the equivalent circuit is made up of five elements that include the solution resistance (Rs), resistance of the oxide layer (Rc), layer constant phase element (CPEc), inductor resistance (RL), and the inductor element (L) [31, 32]. The equivalent circuit for alloy UNS S31600 (Figure 4(b)) is also made up of five elements: the solution resistance (Rs), the resistance of the oxide layer (Rc), the layer constant phase element (CPEc), the charge–transfer resistance of the electrochemical reaction at the interface metal/layer (Rct), and the phase element of the double layer (CPEdl) [33, 34]. The element values are included in Table 2.

3.3. PP Results. The PP plots for UNS S30400 and UNS S31600 immersed at static conditions in EAWA are shown in Figures 5(a) and 5(c). An initial observation of the Tafel plot shape provides a description of anodic and cathodic reactions occurring at the surface [35]. The anodic and cathodic branches of both SSs are similar, with a slight difference in the anodic ones where the corrosion process occurs. It is observed that the slope for UNS S31600 is steeper than that for UNS S30400, indicating a more reactive anodic reaction in the first one. Extrapolating the anodic and cathodic plots yields all the Tafel parameters summarized in Table 3.

The analysis of CPP plots shows the pitting and repassivation potential behavior over the corrosion potential and a

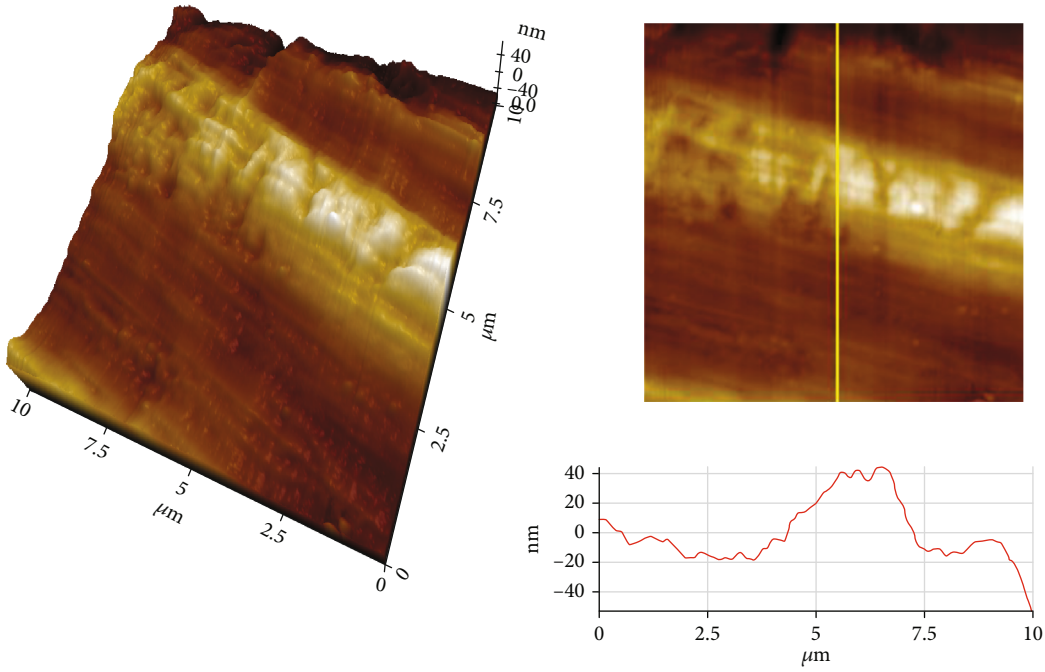

(a)

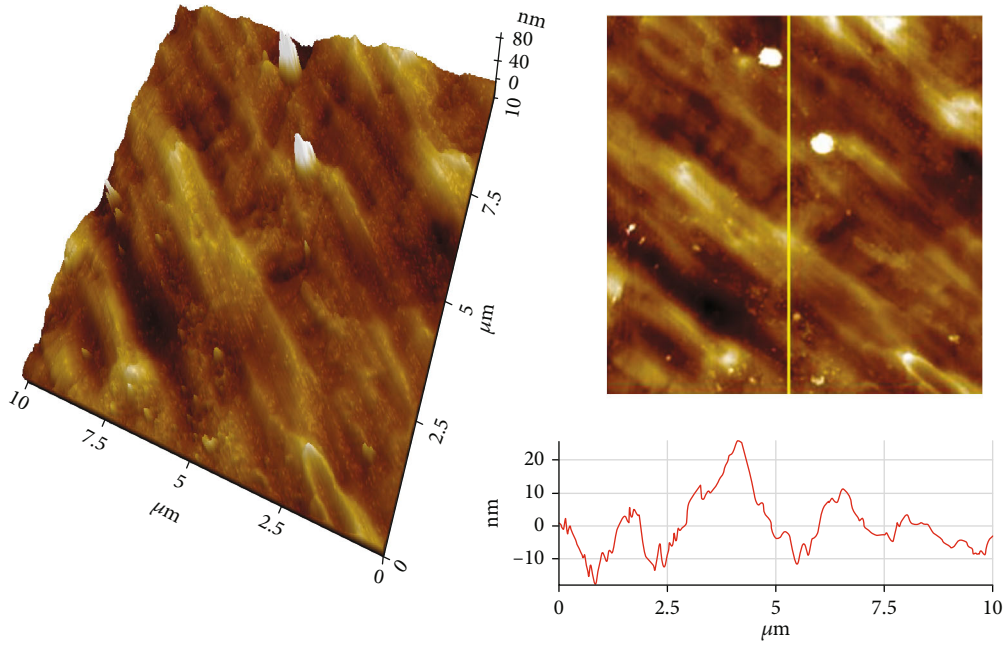

(b)

Figure 8: Continued.

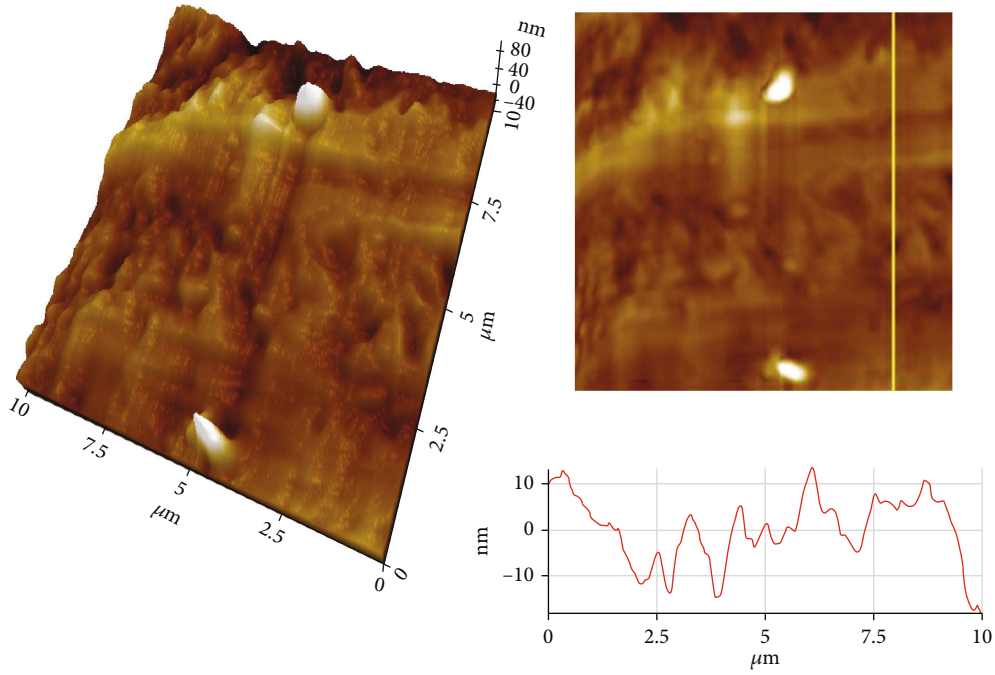

(c)

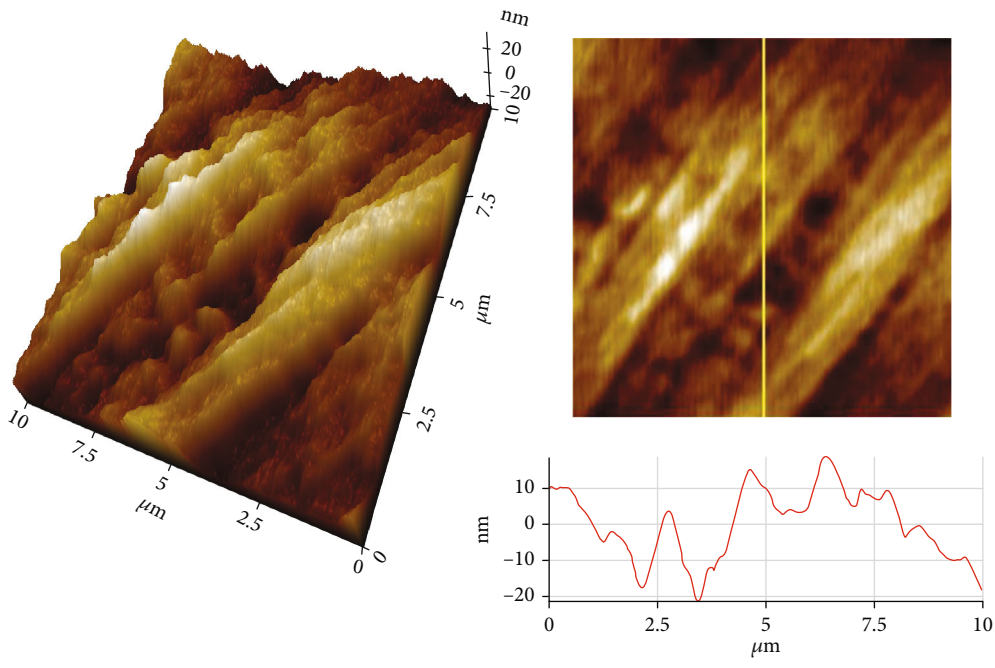

(d)

Figure 8: Continued.

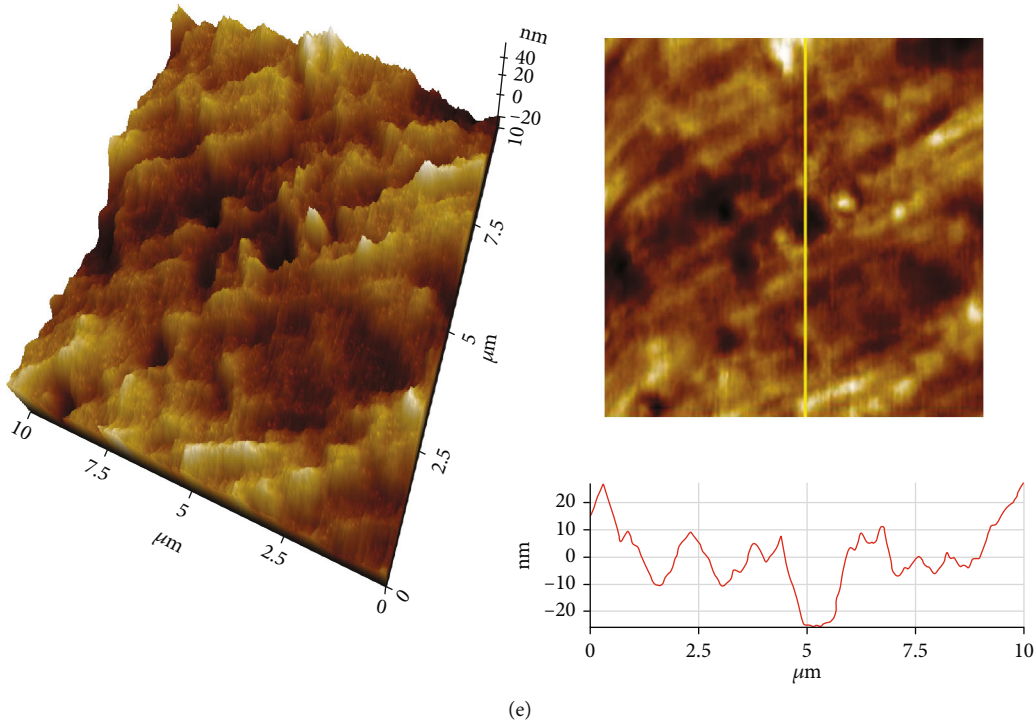

(e)

Figure 8: Representative topographical images, sectional analysis, and AFM tridimensional images of UNS S30400 samples at (a) 0 week, (b) 1 week, (c) 2 weeks, (d) 3 weeks, and (e) 4 weeks of immersion in EAWA.

small hysteresis loop very similar for both SSs (Figures 5(b) and 5(d)). The shape of the curves does not permit to appreciate a clear passivation or transpassivation zone, while the small hysteresis loops in a short negative range. Following the back scan of the hysteresis loop, pass to the positive section, indicating the possibility of passivation for the SS. Nevertheless, this layer is weak and has lost its corrosion protection capacity [36–38]. A clear difference for both SSs is observed in the hysteresis loop at the positive section, with a higher value for UNS S31600 with respect to UNS S30400.

An interpretation of this behavior given by Sun et al. [39], which is interesting due to the EIS results, is that the hysteresis loop is related to the topography of the pit or has sufficient diffusion length. Another critical point to analyze in CPP curves is the difference between the cathodic–anodic transition (EF) and the anodic–cathodic transition (EB). In both SSs, the curves had a nobler cathodic–anodic transition, so the material has difficulty in stopping or cannot stop the localized attack once it has started [36].

3.4. Surface Analysis. Figures 6 and 7 show the micrographs obtained by SEM of the SS samples immersed in EAWA for 1, 2, 3, and 4 weeks. For sample UNS S30400, the pits along the surface increase over time, which has been noticeable since Week 1. In Week 4, the pits along the surface increase in size, finding points where the pits have fused. On the other hand, UNS S31600 also shows pitting, but with a different behavior. Pitting also appeared in Week 1; however, pitting on the surface is minor.

Interestingly, some pits are located at the grain boundaries. Therefore, the superficial analysis agrees with the description mentioned above. In addition, EDS analysis by points shows the chemical composition of the SS surfaces. For both SSs, pits are composed of product oxides and nonmetallic inclusions.

The sample surfaces were analyzed by AFM to know the depth, diameter, shape of pitting, and roughness profiles [40–42]. Bidimensional, tridimensional, and section analysis of pits by AFM images are shown in Figures 8 and 9 for both SS samples exposed during 1–4 weeks. Sectional analysis reveals that topography was modified proportionally to the exposure time, with evidence of pitting since Week 3. The diameter, depth, and shape of the pits vary considerably after Week 4, with diameters lower than 1 μm and a maximum depth of 25 nm for UNS S30400, while in UNS S31600, diameters are higher than 2 μm and 70 nm deep. The results agree with the pitting process predicted by the PP curves, and for UNS S31600, pits are located at the grain boundaries.

4. Discussion

EAWA represents an interesting alternative for general disinfection and fomites, demonstrating a superior antimicrobial spectrum compared to other commonly used chemical disinfectants [12]. EAWA is easy to prepare and cheap, making it a perfect alternative to eliminate resistant microorganisms [43–47]. SSs, UNS S30400 and UNS S31600, used as materials for medical instrument and equipment manufacturing, showed corrosion resistance when exposed to EAWA according to the corrosion rates. However, they are susceptible to pitting corrosion after prolonged exposure.

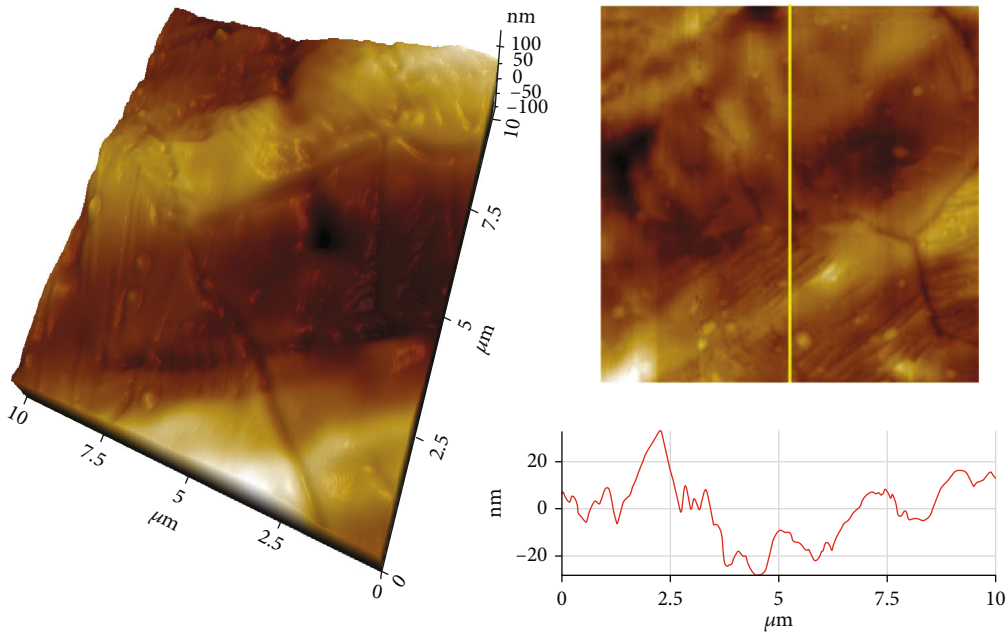

(a)

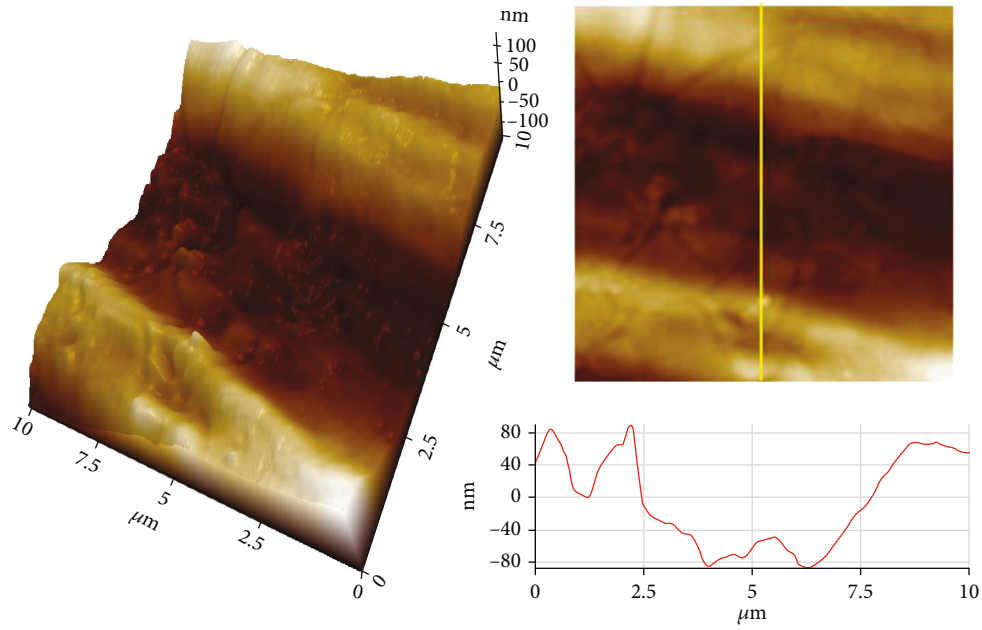

(b)

Figure 9: Continued.

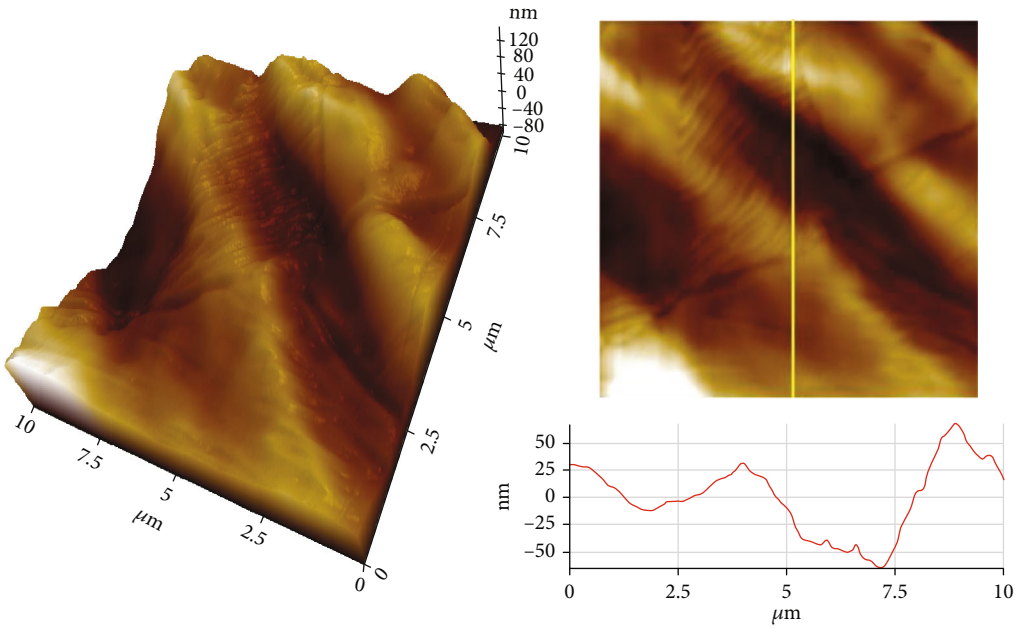

(c)

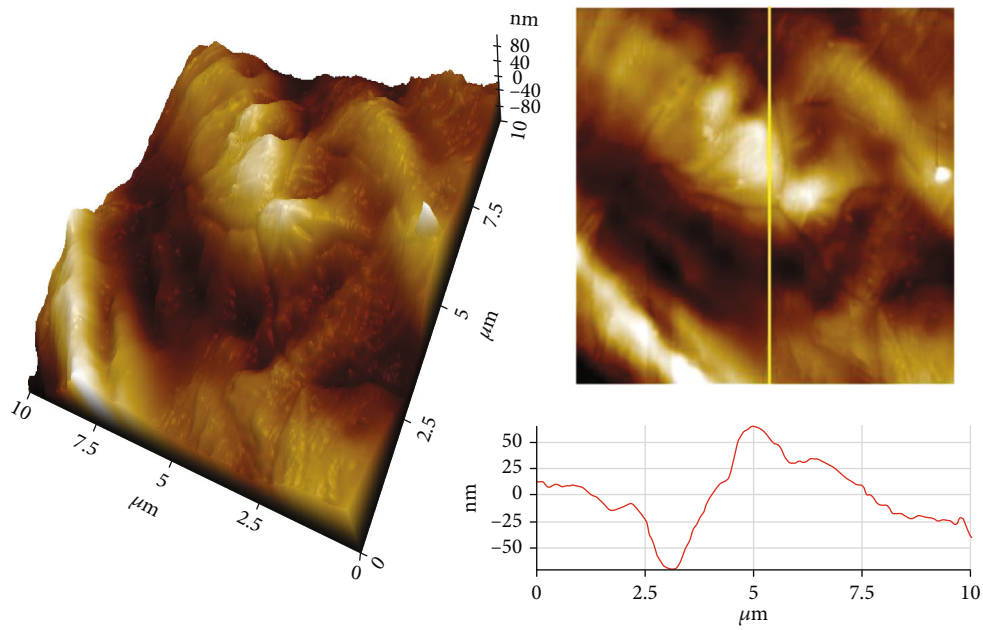

(d)

Figure 9: Continued.

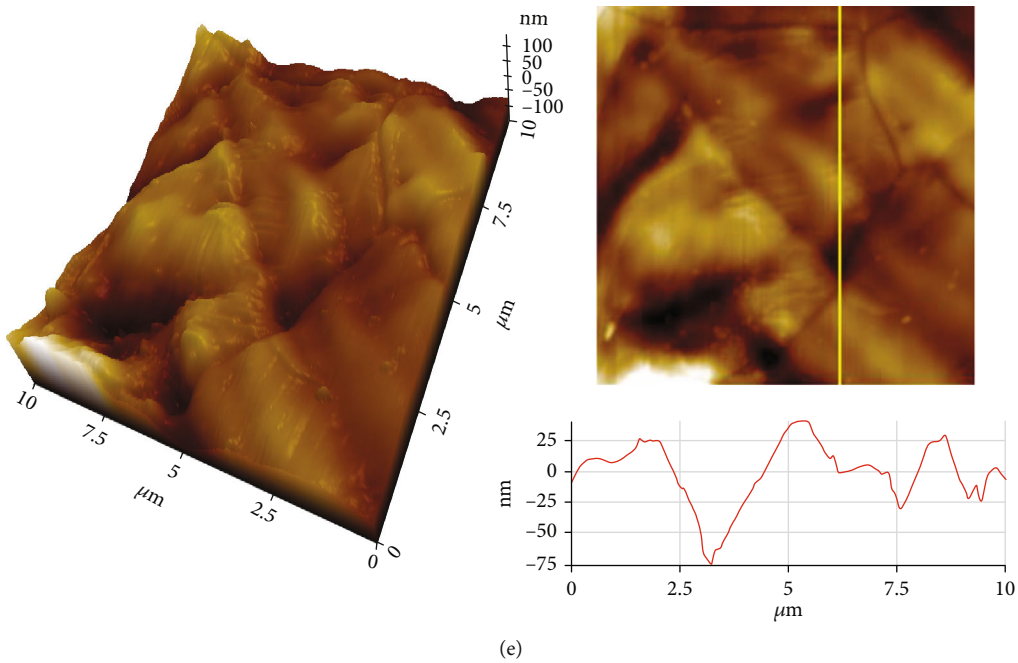

(e)

Figure 9: Representative topographical images, sectional analysis, and AFM tridimensional images of UNS S31600 samples at (a) 0 week, (b) 1 week, (c) 2 weeks, (d) 3 weeks, and (e) 4 weeks of immersion in EAWA.

EAWA has been used in hospital disinfection of surfaces for several decades and is a standard product in the Asian market [48]. The antimicrobial effectiveness is due to the different physicochemical parameters such as the ORP and pH values and the concentration of active chemical species containing oxygen and chlorine to yield compounds such as HOCl. Another critical factor is the contact or exposure time between the metallic surfaces and the EAWA. Different reports in microbiological tests show that a range from 1 to 10 min has been established for concentrations varying from 48 to 109 ppm [49–51].

Corrosion rates from gravimetric and electrochemical polarization corrosion tests showed better corrosion resistance for UNS S31600 compared to UNS S30400 under the corrosion criteria of NACE RP0775-2005 [22]. In addition, we observed a low corrosion rate of <0.025 mm per year for both alloys. On the other hand, following the Fontana criteria [52], UNS S30400 has excellent corrosion resistance, and UNS S31600 has outstanding behavior. According to these corrosion grade classifications, EAWA is not aggressive toward SS instruments and medical devices at short exposure times.

The potential corrosion damage to SS exposed to EAWA comes from the chlorine raw material used for production. The presence of chloride ions in this solution and the pH range from 2 to 5.5 [14, 53] promote its corrosiveness. The EAWA solution used in this research contains the following species: HClO, HO_2*, Cl_2, and HCl, and their equilibrium depends on the pH value between 4 and 5 when all the Cl_2 is present as HClO, which is our case where the pH was 4.5 ± 0.2. Compared to corrosion rate values reported in other works, we could note that EAWA is less aggressive toward SSs than common chloride aqueous solutions [23–25].

Surface analysis by SEM, EDS, and AFM on SS samples exposed to EAWA for 4 weeks gave evidence of pitting corrosion. These results agree with the electrochemical tests. EIS plots showed different responses for the evaluated SS, where UNS S30400 is more susceptible to pitting corrosion, while UNS S31600 showed an incomplete semicircle due to the formation of a more resistant layer but not enough to avoid pitting progress as it was demonstrated in the CPP analysis. The results from the CPP electrochemical tests also indicate a pitting corrosion process occurring at the surface of both SSs, which is more aggressive toward UNS S30400.

5. Conclusions

Both SSs, UNS S30400 and UNS S31600, exposed to acidic anolyte EAWA with an ORP of 1100 ± 15 mV and a pH of 4.5 ± 0.2, were susceptible to localized pitting corrosion. Short exposure times showed good viability for the use of EAWA in the disinfection of medical instruments and devices and SS work surfaces in clinical installations. According to the corrosion rate and criteria established by Fontana and NACE RP0775-2005, both SSs can have outstanding corrosion resistance behavior if long contact times between EAWA and metallic surfaces are avoided. After the disinfection with EAWA, SS surfaces must be rinsed with distilled water to remove most of the aggressive residues.

Data Availability Statement

The data that support the findings of this study are available from the corresponding author upon reasonable request.

Conflicts of Interest

The authors declare no conflicts of interest.

Funding

This research was funded by the SEP-CONACYT Program (No. 317330 FOP02 CONACYT). This work was supported by the CONACYT, Mexico.

Acknowledgments

This work was supported by the CONACYT, Mexico.

References

[1] V. M. Bakhir, "On the nature of electrochemical activation of media," *Reports of the USSR Academy of Sciences*, vol. 286, pp. 663–666, 1986.

[2] I. Ignatov, G. Gluhchev, S. Karadzhov, G. Miloshev, N. Ivanov, and O. Mosin, "Preparation of electrochemically activated water solutions (catholyte/anolyte) and studying their physical-chemical properties," *Journal of Medicine, Physiology and Biophysics.*, vol. 11, pp. 1–21, 2015.

[3] S.-Y. Hsu, "Effects of flow rate, temperature and salt concentration on chemical and physical properties of electrolyzed oxidizing water," *Journal of Food Engineering*, vol. 66, no. 2, pp. 171–176, 2005.

[4] S. Van Haute, B. Zhou, Y. Luo, I. Sampers, M. Vanhaverbeke, and P. Millner, "The use of redox potential to estimate free chlorine in fresh produce washing operations: possibilities and limitations," *Postharvest Biology and Technology*, vol. 156, article 110957, 2019.

[5] I. I. Gluhchev, S. K. Miloshev, and N. I. Mosin, "The evaluation of the mathematical model of interaction of electrochemically activated water solutions (anolyte and catholyte) with water," *European Reviews of Chemical Research*, vol. 4, no. 2, pp. 72–86, 2015.

[6] K. Ghebremichael, E. Muchelemba, B. Petrusevski, and G. Amy, "Electrochemically activated water as an alternative to chlorine for decentralized disinfection," *Journal of Water Supply: Research and Technology—Aqua*, vol. 60, no. 4, pp. 210–218, 2011.

[7] V. Ptashnyk, I. Bordun, V. Pohrebennyk, S. Ziembowicz, M. Kida, and P. Koszelnik, "Aspects of electrochemically activated water solutions practical use," *Journal of Ecological Engineering*, vol. 21, no. 7, pp. 222–231, 2020.

[8] M. S. Block and B. G. Rowan, "Hypochlorous acid: a review," *Journal of Oral and Maxillofacial Surgery*, vol. 78, no. 9, pp. 1461–1466, 2020.

[9] G. Gluhchev, I. Ignatov, S. Karadzhov, G. Miloshev, N. Ivanov, and O. Mosin, "Electrochemically activited water: biophysical and biological effects of anolyte and catholyte types of water," *European Journal of Molecular Biotechnology*, vol. 7, no. 1, pp. 12–26, 2015.

[10] H.-J. Kim, C. N. Tango, R. Chelliah, and D.-H. Oh, "Sanitization efficacy of slightly acidic electrolyzed water against pure cultures of Escherichia coli, Salmonella enterica, Typhimurium, Staphylococcus aureus and Bacillus cereus spores, in comparison with different water hardness," *Scientific Reports*, vol. 9, no. 1, p. 4348, 2019.

[11] J. Salvador Carlos, B. Valdez Salas, E. A. Beltran Partida, M. Curiel Alvarez, N. Cheng, and E. Valdez Salas, "Rapid optimization of disinfectants by photographic image-based analysis and design of experiments," *DYNA*, vol. 99, no. 2, pp. 154–158, 2024.

[12] World Health Organization (WHO), "Hypochlorous acid – disinfection, antisepsis, wound care," 2024, https://www.who.int/groups/expert-committee-on-selection-and-use-of-essential-medicines/23rd-expert-committee/a18-hypochlorous (accessed Aug. 20, 2024).

[13] A. Iram, X. Wang, and A. Demirci, "Electrolyzed oxidizing water and its applications as sanitation and cleaning agent," *Food Engineering Reviews*, vol. 13, no. 2, pp. 411–427, 2021.

[14] P. Yan, E. B.-M. Daliri, and D.-H. Oh, "New clinical applications of electrolyzed water: a review," *Microorganisms*, vol. 9, no. 1, p. 136, 2021.

[15] G. Robinson, R. Thorn, and D. Reynolds, "The effect of long-term storage on the physiochemical and bactericidal properties of electrochemically activated solutions," *International Journal of Molecular Sciences*, vol. 14, no. 1, pp. 457–469, 2013.

[16] X. T. Xuan, M. M. Wang, J. Ahn et al., "Storage stability of slightly acidic electrolyzed water and circulating electrolyzed water and their property changes after application," *Journal of Food Science*, vol. 81, no. 3, pp. E610–E617, 2016.

[17] B. Ayebah and Y. Hung, "Electrolyzed water and its corrosiveness on various surface materials commonly found in food processing facilities," *Journal of Food Process Engineering*, vol. 28, no. 3, pp. 247–264, 2005.

[18] N. Tanaka, T. Fujisawa, T. Daimon et al., "The effect of electrolyzed strong acid aqueous solution on hemodialysis equipment," *Artificial Organs*, vol. 23, no. 12, pp. 1055–1062, 1999.

[19] R. H. Katzenberger, A. Rösel, and R.-P. Vonberg, "Bacterial survival on inanimate surfaces: a field study," *BMC Research Notes*, vol. 14, no. 1, p. 97, 2021.

[20] R. Lagha, M. N. Bellon-Fontaine, M. Renault et al., "Impact of long-term starvation on adhesion to and biofilm formation on stainless steel 316 L and gold surfaces of *Salmonella enterica* serovar Typhimurium," *Annals of Microbiology*, vol. 65, no. 1, pp. 399–409, 2015.

[21] ASTM and G1-03, "Standard Practice for Preparing, Cleaning, and Evaluating Corrosion Test Specimens," 2012, https://www.astm.org/g0001-03.html.

[22] NACE RP-775, *Standard Recommended Practice Preparation, Installation, Analysis, and Interpretation of Corrosion Coupons in Oilfield Operations*, Scientific Research Publishing, 2016, https://www.scirp.org/reference/referencespapers?referenceid=1890163 (accessed Aug. 20, 2024).

[23] P. Dhaiveegan, N. Elangovan, T. Nishimura, and N. Rajendran, "Corrosion behavior of 316L and 304 stainless steels exposed to industrial-marine-urban environment: field study," *RSC Advances*, vol. 6, no. 53, pp. 47314–47324, 2016.

[24] Z. H. Jin, H. H. Ge, W. W. Lin, Y. W. Zong, S. J. Liu, and J. M. Shi, "Corrosion behaviour of 316L stainless steel and anti-corrosion materials in a high acidified chloride solution," *Applied Surface Science*, vol. 322, pp. 47–56, 2014.

[25] A. Ul-Hamid, H. Saricimen, A. Quddus, A. I. Mohammed, and L. M. Al-Hems, "Corrosion study of SS304 and SS316 alloys in atmospheric, underground and seawater splash zone in the Arabian Gulf," *Corrosion Engineering, Science and Technology*, vol. 52, no. 2, pp. 134–140, 2017.

[26] N. O. Laschuk, E. B. Easton, and O. V. Zenkina, "Reducing the resistance for the use of electrochemical impedance spectroscopy analysis in materials chemistry," *RSC Advances*, vol. 11, no. 45, pp. 27925–27936, 2021.

[27] D. Klotz, "Negative capacitance or inductive loop?–A general assessment of a common low frequency impedance feature," *Electrochemistry Communications*, vol. 98, pp. 58–62, 2019.

[28] M. A. Maleeva, A. A. Rybkina, A. I. Marshakov, and V. V. Elkin, "The effect of atomic hydrogen on the anodic dissolution of iron in a sulfate electrolyte studied with impedance spectroscopy," *Protection of Metals*, vol. 44, no. 6, pp. 548–556, 2008.

[29] H. Schweickert, W. J. Lorenz, and H. Friedburg, "Impedance measurements of the anodic iron dissolution," *Journal of the Electrochemical Society*, vol. 127, no. 8, pp. 1693–1701, 1980.

[30] M. de Pauli, A. M. Gomes, R. L. Cavalcante et al., "Capacitance spectra extracted from EIS by a model-free generalized phase element analysis," *Electrochimica Acta*, vol. 320, article 134366, 2019.

[31] Q. Qu, L. Wang, L. Li, Y. He, M. Yang, and Z. Ding, "Effect of the fungus, Aspergillus niger, on the corrosion behaviour of AZ31B magnesium alloy in artificial seawater," *Corrosion Science*, vol. 98, pp. 249–259, 2015.

[32] M. Sun, A. Yerokhin, M. Y. Bychkova, D. V. Shtansky, E. A. Levashov, and A. Matthews, "Self-healing plasma electrolytic oxidation coatings doped with benzotriazole loaded halloysite nanotubes on AM50 magnesium alloy," *Corrosion Science*, vol. 111, pp. 753–769, 2016.

[33] J. Soto Puelles, M. Ghorbani, R. Yunis et al., "Electrochemical and surface characterization study on the corrosion inhibition of mild steel 1030 by the cationic surfactant cetrimonium trans-4-hydroxy-cinnamate," *ACS Omega*, vol. 6, no. 3, pp. 1941–1952, 2021.

[34] M. Zhang, H. Wang, T. Nie, J. Bai, F. Zhao, and S. Ma, "Enhancement of barrier and anti-corrosive performance of zinc-rich epoxy coatings using nano-silica/graphene oxide hybrid," *Corrosion Reviews*, vol. 38, no. 6, pp. 497–513, 2020.

[35] M. Stern and A. L. Geary, "Electrochemical polarization: I. A theoretical analysis of the shape of polarization curves," *Journal of the Electrochemical Society*, vol. 104, no. 1, p. 56, 1957.

[36] S. Esmailzadeh, M. Aliofkhazraei, and H. Sarlak, "Interpretation of cyclic potentiodynamic polarization test results for study of corrosion behavior of metals: a review," *Protection of Metals and Physical Chemistry of Surfaces*, vol. 54, pp. 976–989, 2018.

[37] M. Finšgar, S. Fassbender, F. Nicolini, and I. Milošev, "Polyethyleneimine as a corrosion inhibitor for ASTM 420 stainless steel in near-neutral saline media," *Corrosion Science*, vol. 51, no. 3, pp. 525–533, 2009.

[38] M. Finšgar, S. Fassbender, S. Hirth, and I. Milošev, "Electrochemical and XPS study of polyethyleneimines of different molecular sizes as corrosion inhibitors for AISI 430 stainless steel in near-neutral chloride media," *Materials Chemistry and Physics*, vol. 116, no. 1, pp. 198–206, 2009.

[39] D. Sun, Y. Jiang, Y. Tang et al., "Pitting corrosion behavior of stainless steel in ultrasonic cell," *Electrochimica Acta*, vol. 54, no. 5, pp. 1558–1563, 2009.

[40] P. Leblanc and G. S. Frankel, "A study of corrosion and pitting initiation of AA2024-T3 using atomic force microscopy," *Journal of the Electrochemical Society*, vol. 149, no. 6, p. B239, 2002.

[41] J. Li, "In-situ AFM study of pitting corrosion of Cu thin films," *Colloids and Surfaces A: Physicochemical and Engineering Aspects*, vol. 154, no. 1-2, pp. 227–237, 1999.

[42] I. Reynaud-Laporte, M. Vayer, J.-P. Kauffmann, and R. Erre, "An electrochemical-AFM study of the initiation of the pitting corrosion of a martensitic stainless steel," *Microscopy Microanalysis Microstructures*, vol. 8, no. 3, pp. 175–185, 1997.

[43] R. I. Farah and S. N. Al-Haj Ali, "Electrolyzed water generated on-site as a promising disinfectant in the dental office during the COVID-19 pandemic," *Frontiers in Public Health*, vol. 9, article 629142, 2021.

[44] X. X. Hao, B. M. Li, C. Y. Wang, Q. Zhang, and W. Cao, "Application of slightly acidic electrolyzed water for inactivating microbes in a layer breeding house," *Poultry Science*, vol. 92, no. 10, pp. 2560–2566, 2013.

[45] M. Kurahashi, T. Ito, and A. Naka, "Spatial disinfection potential of slightly acidic electrolyzed water," *PLoS One*, vol. 16, no. 7, article e0253595, 2021.

[46] H. F. van Dijk and H. A. Verbrugh, "Resisting disinfectants," *Communications Medicine*, vol. 2, no. 1, p. 6, 2022.

[47] L. Zhao, S. Li, and H. Yang, "Recent advances on research of electrolyzed water and its applications," *Current Opinion in Food Science*, vol. 41, pp. 180–188, 2021.

[48] B.-K. Chen and C.-K. Wang, "Electrolyzed water and its pharmacological activities: a mini-review," *Molecules*, vol. 27, no. 4, p. 1222, 2022.

[49] J. W. Buck, M. W. Van Iersel, R. D. Oetting, and Y.-C. Hung, "In vitro fungicidal activity of acidic electrolyzed oxidizing water," *Plant Disease*, vol. 86, no. 3, pp. 278–281, 2002.

[50] X. Cheng, Y. Tian, C. Zhao et al., "Bactericidal effect of strong acid electrolyzed water against flow enterococcus faecalis biofilms," *Journal of Endodontics*, vol. 42, no. 7, pp. 1120–1125, 2016.

[51] Y. Takeda, H. Uchiumi, S. Matsuda, and H. Ogawa, "Acidic electrolyzed water potently inactivates SARS-CoV-2 depending on the amount of free available chlorine contacting with the virus," *Biochemical and Biophysical Research Communications*, vol. 530, no. 1, pp. 1–3, 2020.

[52] M. G. Fontana, "Corrosion Engineering," in *McGraw Hill Series in Materials Science and Engineering*, McGraw Hill, New York, 3rd edition, 1986.

[53] U. K. Mudali and M. G. Pujar, "Pitting corrosion of austenitic stainless steels and their weldments," in *Corrosion of Austenitic Stainless Steels*, pp. 74–105, Elsevier, 2002.